Chapter 2

Beam Test of a Prototype SCT Module

As already pointed out in the previous chapter, beam tests form the backbone of the detector element evaluation process. This chapter documents one particular beam test carried out with a p^+ on n type silicon strip detector equipped with analogue read-out electronics. The true goal of the beam test was to test the analogue read-out chip SCTA128HC, as well as to perform a cross-check on the performance of the detector. The components under test and the experimental setup are described. Then the results of the analysis of the data collected in the beam test are presented.

2.1 Silicon strip detectors in ATLAS

The ATLAS SCT aims to operate reliably, according to the performance specifications, over a 10 year period of the high luminosity LHC operation. As the detectors will be exposed to fluencies 10-20 times higher than in past applications, a substantial development effort has been made to ensure adequate radiation resistance in the design. Additionally, the SCT's active area is $\sim 63\,\mathrm{m}^2$, more than 50 times that of any existing silicon vertex detector. It extends over 1 m in diameter and 6 m in length, again posing challenges to the detector services, cooling and precision mechanics techniques.

As the SCT is sub-detector of the ID, the physics requirements for the SCT can be projected from those for the ID by taking into account the pixel detector and TRT capabilities. The main points that can be extracted are:

- The required reconstruction efficiency requirement for isolated leptons of $p_T > 5\,\mathrm{GeV}$ to have an efficiency of 95% and a fake track rate $< 1\%$, imposes the need to reconstruct helices in 3D, especially since the TRT provides no r/z measurement. Thus we need at least six tracking layers providing full space point information, and a detector efficiency above 95% over the whole lifetime of the experiment to ensure good tracking and trigger efficiency. The upper limit on fake rate also determines the noise occupancy of the detector.

- The requirement that $\delta p_T/p_T < 0.3$ at $p_T = 500\,\mathrm{GeV}$ with a beam constraint imposes an r-φ measurement with a resolution of $\sim 20\,\mu$m at the SCT radius. The requirement to separate multiple vertices within a bunch crossing imposes an accuracy on the z

measurement of $< 1\,\text{mm}$ in the SCT. For K^0 reconstruction this resolution should be even better.

- The requirement of a two–track resolution to be $< 200\,\mu\text{m}$ at $r = 30\,\text{cm}$, in order to minimize track losses in b-jets, also constrains the r-φ pitch.

- To minimise material effects preceding the calorimeter, the SCT and pixel layers must have a minimal radiation length. The design aim was to reach $< 0.2X_0$ preceding the TRT over a significant η range.

It would be a duplication of effort to go into all details of detector type and electronics selection. An overview of the studies performed can be found in [7]:Ch:11.

2.1.1 Detectors

A short overview of the current baseline solution is presented. It has already been changed with respect to the one presented in the TDR [5], namely the type of the detector has been changed from n^+ on n to p^+ on n, mainly to decrease cost of production.

The baseline detectors are of the p^+ on n variety, capacitively-coupled with polysilicon biasing. The detector thickness is $260\pm 10\,\mu\text{m}$ (inner barrel and inner wheel) and $285\pm 15\,\mu\text{m}$ otherwise. The barrel modules are 64 mm long and 63.6 mm wide. Forward modules have tapered strips and five slightly different designs are needed to optimally cover the desired space (variations in size with respect to the barrel module remain $< 20\%$). All detectors have a pitch of $80\,\mu\text{m}$ (this is also the central value for the wedge detectors) and 768 read-out strips.

Modules are composed out of two detectors joined one after another, to give 128 mm in length. While this introduces some problems with alignment, the cost consideration has the final word (the detectors are optimised for production from 4" wafers). As each SCT layer must provide a space point per, two half-modules are glued together back-to-back with a 40mrad stereo angle. The complete module is installed with a 10° tilt angle for hermeticity and to compensate for the Lorentz angle.

The operational temperature of the detectors will be $< -7^\circ\,\text{C}$. A low operating temperature is required to reduce the noise due to leakage current and minimise effects of radiation damage.

2.1.2 Read-out electronics

The SCT read-out electronics is responsible for supplying strip hit information to the second level trigger and the data acquisition system. The low signal yields of the silicon micro-strip detectors and the 25 ns shaping time necessitate that the front-end electronics be mounted directly at the silicon strip electrodes to ensure the low noise operation required. This dictates that the electronics must be of low mass and low power consumption. Of course, it must also survive the radiation environment at the LHC. The performance of the detectors combined with that of the electronics must meet the goals of the SCT specifications. A detailed discussion can be found in [7]:Sec:11.4. Here there are only the parameters that are directly connected with the beam test.

The efficiency of the read-out system must be above 99%. The combined efficiency of detector plus electronics must be 97% in order to meet the six space point requirement for the ID. **The noise** should not be larger than $1500e^{-}$. For silicon strip detectors with read-out electronics that has a short shaping time, the strip capacitance is the dominant source of noise. A typical equivalent noise charge of 600-800e^{-} (before irradiation) is a typical value for the detector choices considered by ATLAS. The upper limit on **noise occupancy** is set to 5×10^{-4}. This should be compared to an average occupancy of 0.6% during high luminosity operation and a 2-3% occupancy in b-jets.

With respect to the level 1 trigger additional requirements are imposed. The electronics should store the data for the maximum latency of the level 1 trigger (2.5 μs plus 0.5 μs for signal dispatching which corresponds to 120 bunch crossings). It should be able to operate with the average level 1 rate of 100 kHz. As this includes the read-out time, eight more memory locations are needed in the buffer to store selected events before they can be read-out.

While binary read-out is the present baseline, both analogue and binary versions of the read-out electronics are, being pursued. Various chip architectures have been designed and tested at different levels. Only few of them have made it to the final trial of being placed in the test beam, as part of a full prototype module.

2.1.3 SCTA128HC read-out chip

A detailed description of the SCTA128HC read-out chip and its performance has been published [15]. Here only a brief overview and a few details that particularly affect the measurements are presented.

The chip was designed to provide support for 128 read-out strips with capacitance from 0 to 25pF. Besides the control logic, the main components of the chip are the front-end amplifiers, the analogue data pipeline and the output multiplexer. The front-end block consists of a bipolar amplifier followed by a shaper providing a semi-Gaussian shaping ($CR-RC^2$) with a peaking time of 25 ns. The peak values are sampled at 40 MHz and stored in the 128-cell deep analogue buffer. Another 8-cell circular buffer is provided to store pointers to cells that were marked by the trigger. The time offset of the trigger signal can be set in internal clock units to allow for different trigger latencies. Upon receiving a trigger signal the data is sent out via a fast 40 MHz analogue multiplexer, which can also operate at a reduced rate of 20, 10 and 5 MHz.

The gain is linear for charges of up to 12fC (1fC $\sim 6240e^{-}$) with an average gain of 25.5 mV/ fC and a 2% error. As a reference point note that a minimum ionizing particle produces a charge of 3.5fC (most probable value, $\sim 21\,800e^{-}$) when passing through 280 μm of silicon. The pedestal variation from channel to channel is typically $\sim$ 25 mV, but this doesn't influence the measurements. More important is the variation along the pipeline (for a single channel), which has a rms variation of 1.2 mV or $300e^{-}$.

2.2 Experimental setup

The beam test was performed with 200 GeVpions at CERN in the X5 west area of the SPS (for a more detailed description of the beam infrastructure see [16]). The module was installed in the beam telescope of the RD42 group. Their readout system was modified to provide a common data output.

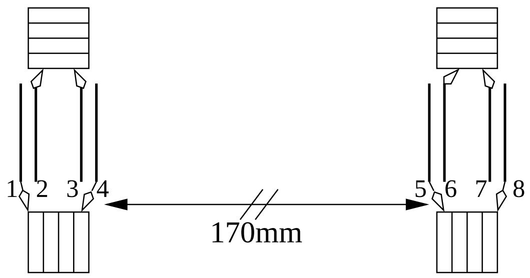

Figure 2.1: A schematic view of the beam telescope. Dashed boxes show orientations of telesope planes.

Plane ID	position	tilt	pitch	interpolation strips
1	$-95\,\mathrm{mm}$	$0°$	$50\,\mu\mathrm{m}$	2
2	$-93\,\mathrm{mm}$	$90°$	$50\,\mu\mathrm{m}$	2
3	$-87\,\mathrm{mm}$	$90°$	$50\,\mu\mathrm{m}$	2
4	$-85\,\mathrm{mm}$	$0°$	$50\,\mu\mathrm{m}$	2
5	$85\,\mathrm{mm}$	$0°$	$50\,\mu\mathrm{m}$	1
6	$87\,\mathrm{mm}$	$90°$	$50\,\mu\mathrm{m}$	1
7	$93\,\mathrm{mm}$	$90°$	$50\,\mu\mathrm{m}$	1
8	$95\,\mathrm{mm}$	$0°$	$50\,\mu\mathrm{m}$	1

Table 2.1: Beam telescope specifications

2.2.1 Beam telescope

The beam telescope used was composed of 8 single-sided silicon strip detectors installed over a distance of 19 cm. The dimensions of the detectors were $12.8\,\mathrm{mm} \times 12.8\,\mathrm{mm} \times 300\,\mu\mathrm{m}$ and each had 256 read-out strips connected to the VIKING read-out hybrid. All telescope modules had interpolation strips (one half of the detectors had two and the other half a single one) which enable capacitive sharing between the read-out strips. Combined with a high signal to noise ratio of these devices this enables one to reliably reconstruct the intersection position using the *eta* method (discussed in Sec:2.4.2). A schematic view of the beam telescope is shown in Fig:2.1 and Tab:2.1 gives the important data. The typical cluster sizes and their signal to noise ratios are presented in Fig:2.2.

For our purposes the most important parameter of the telescope is its resolution at the point where our device under test is placed in the beam. The first step is to understand the intrinsic resolutions of the telescope modules. As the number of interpolation strips changes the module's resolution, one of each kind was excluded from the track fit (one at a time) and its resolution 'measured'. The residual distributions are shown in Fig:2.3. The obtained resolutions are $\sigma_{1-4} = 3.4\,\mu\mathrm{m}$ for the detectors with two interpolation strips and $\sigma_{5-8} = 7.8\,\mu\mathrm{m}$ for the detectors with a single one.

These numbers were used as the basis for a Monte-Carlo simulation which was tuned to give the same residuals on the planes 4 and 5 when their faked measurements were not used in the fit. Details of the procedure are given in App:A. In the same way the intrinsic spatial

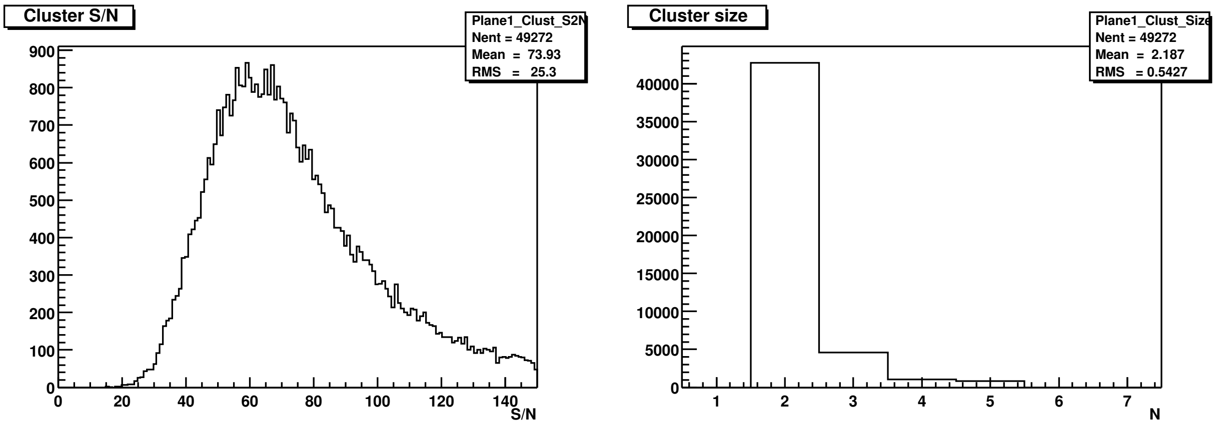

Figure 2.2: Left: the signal to noise ratio for the reconstructed clusters. Right: distribution of a cluster size.

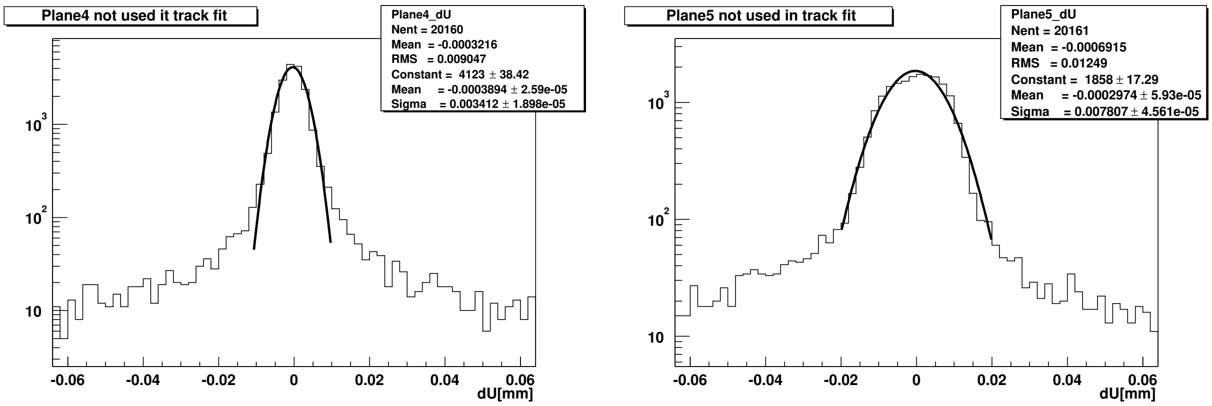

Figure 2.3: The residual distributions of the fourth and fifth telescope plane. For both plots only the plane in question was not used in the track fitting.

resolution of the tracker at plane $z = 0$ was 'measured'. See Fig:2.4. The standard deviation of this residual distribution is the precision of the tracker and *all subsequent resolutions are effectively convoluted with a Gaussian distribution of* $\sigma = 2.5\,\mu$m.

2.2.2 The device under test

The module under test was a standard barrel half-module composed of two p^+ on n AC coupled detectors with $80\,\mu$m pitch and thickness $280\,\mu$m. Their strip width was $25\,\mu$m and strip depth $4\,\mu$m. The two detectors were interconnected in the regions of the second and the fourth chip (strips 129-256 and 385-512) therefore enabling measurements on a 6 cm and 12 cm strip length simultaneously. Four SCTA128HC chips were connected to the strip range 1-512, but in fact only strips in the region 330-460 received hits from the beam. The detectors were operating at room temperature.

The baseline detector is optimised for a binary readout. For analogue readout the pitch would be larger, around $110\,\mu$m. The interpolation strips would also be added to the mask

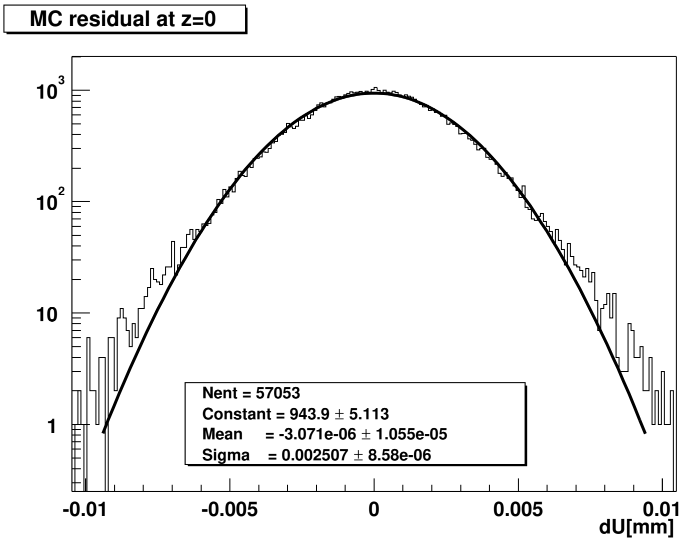

Figure 2.4: The intrinsic tracker residuals at $z = 0$.

of the detector to induce capacitive charge sharing between the read-out strips. Again it must be stressed that the main purpose of this beam test was to assess the quality of the analogue read-out system as well as to make a detailed assessment of detector's response under varying angles of incidence of incoming particles which enables a correct emulation of cluster sizes, noise and resolutions in the large scale simulations of the ATLAS detector.

2.3 Extraction of clusters from raw data

Information about the charge collected on a single strip is presented as a number of ADC counts in the channel representing the relevant strip. Alas, not all the voltage read off the strip electronics is due to amplification of the charge produced in the detector by the passing particle. The silicon detectors are diodes, under reverse bias, which means that in each measurement we necessarily pick up a contribution from the dark current. This contributes to the noise and pedestal. Secondly, internal structure of a read-out electronics (preamplifiers and ground level determination) brings in additional noise, pedestal and common mode pedestal variations. Common mode variations are reasonably defined for a region (or a zone) of a detector which is read-off by the same electronics (in our case: by the same chip).

All things considered, raw signal value on strip i for event n can be expressed as:

$$R_i^n = S_i^n + P_i^n + N_i^n + C_Z^n, \tag{2.1}$$

where R_i^n is the raw value, S_i^n signal, P_i^n pedestal, N_i^n noise and C_Z^n common mode shift for zone Z of which strip i is a member.

It is matter of convention (or even more of taste) how we define pedestal and noise. I choose to add the mean noise value into the pedestal so that noise represents the rms of pedestal variations around its mean value.

Of course the true values of S_i^n, P_i^n, N_i^n and C_Z^n are not known (and to be honest, R_i^n is only known up to the precision of AD conversion). We approximate them by using information from previous events. [1]

2.3.1 Pedestal, noise and common mode determination

The problem is that pedestal, noise and common mode variations are not constant in time. The estimator for pedestal and noise is calculated as a running average over the last $\mathcal{N}_p$ and $\mathcal{N}_n$ events respectively. Common mode variations are calculated on a per event basis.

But in the beginning of the run we know nothing about the pedestal nor noise. To get the estimators for the first event we therefore histogram the raw signals for the first $\mathcal{N}_p$ or $\mathcal{N}_n$ (whichever is greater) events on a per strip basis. Then we fit those distributions with a Gaussian curve and assign the mean value to $\widetilde{P_i^1}$ and the spread to $\widetilde{N_i^1}$.

Now assume that we know the estimators for event n and that we want to calculate the relevant quantities. A first approximation for the signal ($\dot{S_i^n}$) is just the pedestal estimator subtracted from the raw value:

$$\dot{S_i^n} = R_i^n - \widetilde{P_i^n}. \tag{2.2}$$

Next we select only strips with $\dot{S_i^n} < 3\widetilde{N_i^n}$ for common mode determination. Let $\mathcal{A}_Z$ represent a set of such indices for zone Z and calculate:

$$C_Z^n = \frac{\sum_{j\in\mathcal{A}_Z} \dot{S_j^n}}{|\mathcal{A}_Z|}. \tag{2.3}$$

Using this we come to a second and final approximation ($\ddot{S_i^n}$) for the signal:

$$\ddot{S_i^n} = \dot{S_i^n} - C_Z^n \qquad i \in \mathcal{M}_Z, \tag{2.4}$$

where $\mathcal{M}_Z$ is a set of all strips in zone Z. This is the value used for the cluster search and determination of the hit position. The only thing still needed is 'true' noise and pedestal for the calculation of estimators for the next event:

$$\left.\begin{array}{l} P_i^n = \widetilde{P_i^n} + \ddot{S_i^n} = R_i^n - C_Z^n \\ N_i^n = \ddot{S_i^n} \end{array}\right\} \quad i \in \mathcal{A}_Z \quad \text{for both eqs.} \tag{2.5}$$

Note that common mode correction is not followed by the pedestal estimator but is calculated on a per event basis. Taking into account also the common mode correction would require adding C_Z^n to P_i^n (which is equivalent to using R_i^n for P_i^n).

Now we can calculate the pedestal and noise estimators for the next event. Instead of keeping the old values and recalculating the average it is more practical to use a recursive digital filter (IIR).

$$\widetilde{P_i^{n+1}} = pP_i^n + (1-p)\widetilde{P_i^n} \qquad p = \frac{1}{\mathcal{N}_p} \tag{2.6}$$

$$\widetilde{N_i^{n+1}} = \sqrt{n\ddot{S_i^n}^2 + (1-n)\widetilde{N_i^n}^2} \qquad n = \frac{1}{\mathcal{N}_n} \tag{2.7}$$

Again only values for strips which are members of $\mathcal{A}_Z$ are updated. For other strips (which presumably collected some charge in this event) the estimators are kept unchanged for the next event.

[1] A tilde sign above quantities is used to mark them as estimators. Plain symbols are used for the quantities obtained for a particular event.

2.3.2 Clustering

After the signal is corrected for each strip, following the procedure as in Sec:2.3.1, a search is made for clusters of strips exceeding a predetermined signal-to-noise ratio. The definitions for quantities used in the cluster quality determination will be explained here and some practical problems will be addressed.

In the previous subsection we have described how signal S_i and noise N_i on strip i are obtained from the raw data. The event superscript n has been dropped, as it was only relevant for pedestal and noise updating. We will be mostly concerned about the signal to noise ratio of a strip i and of a cluster C of adjacent strips:

$$Q_i = \frac{S_i}{N_i} \tag{2.8}$$

$$Q_C = \sum_{i \in C} \frac{S_i}{N_i}. \tag{2.9}$$

The definition of Q_C is not entirely correct from a statistical point of view but this is the standard definition used in the literature.

A cluster is a contiguous set of strips that satisfies the following criteria:

1. The signal to noise ratio off all strips must be above the *clustering cut* Q^c: $Q_i \geq Q^c$. A typical value of Q^c is 3.

2. The strip with the highest signal to noise ratio (seed strip) is required to have the S/N ratio greater than the *seed cut* Q^s: $Q_{\text{seed}} \geq Q^s$. In our analysis the values of Q^s were in the range from 4 to 5.

3. The size of the cluster $\mathcal{N}_C$ must be within limits $\mathcal{N}^{min} \leq \mathcal{N}_C \leq \mathcal{N}^{max}$. If it is too small, the cluster is discarded. If it is too big, we start cutting on both sides, throwing out strips with worst Q_i until we hit the limit $\mathcal{N}^{max}$. The rationale behind this cut is that at a given angle of incidence the cluster size will be within well defined limits.

4. The sum of the signal collected in the cluster $S_C = \sum_{i \in C} S_i$ must lie within the range $S^{min} \leq S_C \leq S^{max}$. This prevents us from accepting clusters that are entirely due to noise or to read-out errors with a high ADC value.

The last step requirement is usually replaced by a cut on Q_C. In our case the presented method showed better results.

2.3.3 TDC information

In the ATLAS experiment (and at the LHC in general) bunch crossings will occur every 25 ns and the internal clock of the read-out chips will be set to make the measurement at the peak of signal collection. The experimental setup in the beam test did not conform to these requirements which means that events were recorded at random times, not only at the peak of signal collection. To correct for that, additional information was recorded with each event: the time difference from the beginning of the chip's internal clock cycle to the event trigger time with 125 ps resolution. We refer to this value by the name of the electronic circuit providing us with the measurement: *time to digit converter* (TDC). In the data-analysis, we therefore make a calibration run at the beginning to estimate appropriate cuts on the TDC value. See Fig:2.5 for example of the obtained $S_C(t_{\mathrm{TDC}})$ distribution and the cuts chosen. In a limited range this also shows the signal evolution in time.

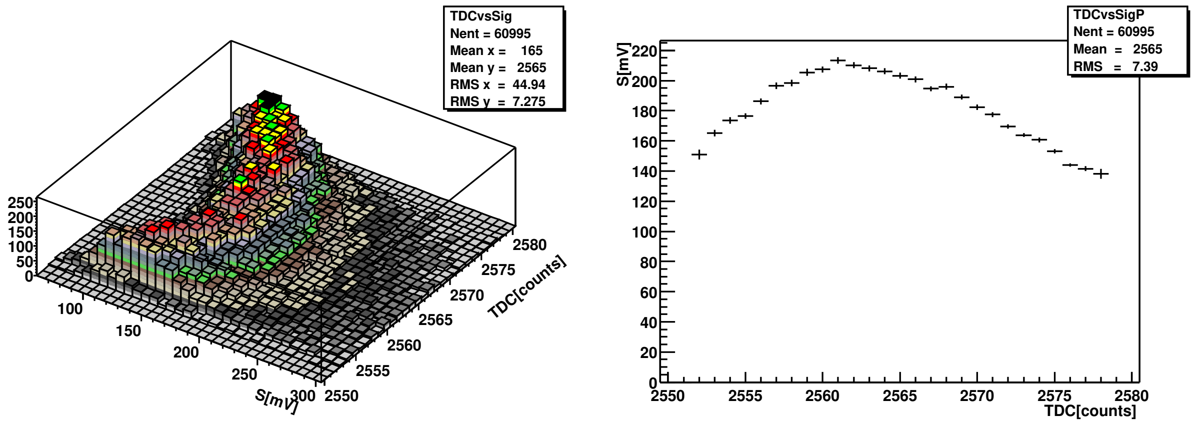

Figure 2.5: Two views of the $S_C(t_{\mathrm{TDC}})$ distribution. The selected cuts were $2559 \leq t_{\mathrm{TDC}} \leq 2566$.

2.4 Determination of cluster position

Having obtained a cluster one still has to determine the track intersection point. There are several possible methods and the relevant ones are presented in this section. Since our detector was being tested at different angles, the cluster size varied accordingly and different methods were used to handle each case. For an overview and a study of the spatial resolution of different position finding algorithms using Monte-Carlo techniques, see [17].

It is time to define a few abbreviations for strip indexes. Let s stand for the seed strip, l for the strip with the lowest index in the cluster and h for the strip with the highest one. Let P denote the pitch (strip to strip distance) of the detector.

In a way the position of the seed strip u_s is the first approximation of the intersection position. Each of the following methods will provide a correction δ_u to this value.

2.4.1 *Centre of gravity* method

This position correction is obtained by weighting the strip position by its signal and calculating the centre of gravity of the cluster.

$$\delta_u^{\mathrm{COG}} = \sum_{l \leq i \leq h} \frac{S_i}{S_C}(i-s)P \tag{2.10}$$

This is the simplest evaluation one can do and can be used as a reference point for evaluating the other methods.

2.4.2 *Eta* method

The eta method is based on the assumption of a ‘flat’ position distribution for incoming particles along the u coordinate. It only works for two–strip clusters under the assumption that in all cases with a given track intersection position between two strips, the charge will get distributed in the same way (but not linearly ... this reduces to the `CoG` method). One 'measures' the distribution of:

$$\eta = \frac{S_L}{S_L + S_R}, \tag{2.11}$$

where L is the 'left' or lower strip index and $R = L + 1$, that is the index of the next neighbouring strip. It can also be used for larger clusters, but then you need to take the seed strip and its neighbour with the highest signal and assign the L, R indexes correctly. This method was used for the telescope detectors where interpolation strips provide capacitive coupling to neighbouring read-out strips.

One then histograms this distribution ($dP/d\eta$) and transforms it to a cumulative one ($\mathcal{P}(\eta) = \int_0^\eta \frac{dP}{d\eta} d\eta$). Here the importance of the flat track distribution comes into the game: if $dP/du = \text{const}$, then $P(\eta)$ gives a position correction in `pitch` units. If $\mathcal{P}(\eta) > 0.5$ this signals that strip R is in fact the seed and that the correction to the seed position should have a negative sign:

$$\delta_u^{\text{eta}} = P \cdot \begin{cases} \mathcal{P}(\eta) & \mathcal{P}(\eta) \le 0.5 \\ \mathcal{P}(\eta) - 1 & \mathcal{P}(\eta) > 0.5 \end{cases} \tag{2.12}$$

2.4.3 *Head–tail* methods

For large clusters such as one obtains with inclined detectors the `eta` method is useless. In cases of a low signal to noise ratio, the `CoG` method is error prone due to noise fluctuations. This leads to the idea of using only strips at cluster boundaries for position correction (called head and tail) and to discard the information from the inner strips altogether. In a way it is a mixture of both previously discussed methods.

The first approximation is called the `digital head-tail` method, which discards the signal information and uses cluster's boundaries only:

$$\delta_u^{\text{DHT}} = \frac{(l-s) + (h-s)}{2} P. \tag{2.13}$$

To further improve it, we must know the average signal S_θ expected on a strip within the cluster. Let S_0^{MP} denote the *most probable* signal collected for a perpendicular track, W its width and P (pitch) its inter-strip distance (Fig:2.6). For an inclined track with incident angle θ its total signal is proportional to the length of track's path through the detector $L = W/\cos\theta$. On the other hand the length of a track under an inner strip equals $P/\sin\theta$. The term inner strip is only relevant when the incident angle of the track is larger than $\tan\theta \ge P/W$ ($\theta \ge 16^\circ$ in our case), i.e., when the track is traversing more than one strip. The expected signal on a strip can then be written:

$$S_\theta = S_0^{\text{MP}} \cdot \begin{cases} \frac{1}{\cos\theta} & \tan\theta < P/W \\ \frac{P}{W\sin\theta} & \tan\theta \ge P/W \end{cases} \tag{2.14}$$

With this we can define the `analogue head-tail` method:

$$\delta_u^{\text{AHT}} = \Big(\frac{(l-s) + (h-s)}{2} + \frac{S_h - S_l}{2S_\theta}\Big) P. \tag{2.15}$$

Therefore we additionally correct the position by the ratio of the measured head/tail signal to the expected one.

Another option, in a way a more general and honest, is to estimate S_θ from the signal collected on the inner strips:

$$\widetilde{S}_\theta = \sum_{l<i<h} \frac{S_i}{h-l-1}. \tag{2.16}$$

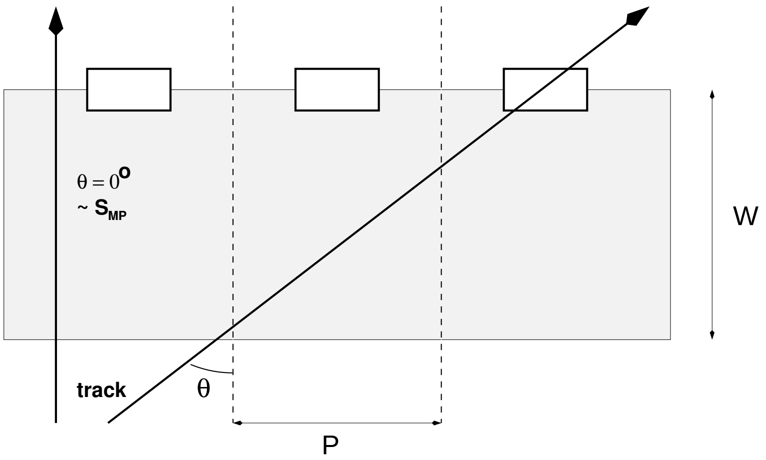

Figure 2.6: Schematic view of track passing through the detector.

2.5 Cluster analysis

Now we are in position to make an educated attack on the data collected in the beam test. A total of six data-sets were analysed, one for each of six different inclinations ranging from 0° to 50° in steps of 10°. For each of those sets we have to further differentiate the read-out channels connected to the 6 cm and 12 cm detectors. All data were collected with the same reverse bias voltage $U = 190\,\mathrm{V}$. The detectors were fully depleted, as the depletion voltage of the detector was measured to be $U_{FD} = 60V$.

For the detector under test, a special alignment procedure was adopted using simplex minimization crossed with the Metropolis algorithm. See Sec:1.3 for details.

2.5.1 Efficiency versus noise occupancy

The first thing one asks is how efficient is the detector. Here there is a bit of a problem: any cluster finding algorithm is subjected to certain cuts and by lowering our requirements for cluster quality one can easily make a detector 100% efficient. But this is not exactly the point here because by lowering the cuts one finds additional clusters that are entirely due to noise. This is quantified by `noise occupancy` which is the number of strips introduced by noise per number of all strips per event. The problem is that one wants the best efficiency with as few noise clusters as possible and that one generally can't have both. Finding out where we stand with our detector in this respect is the goal of this section.

The efficiency and occupancy were histogrammed versus a Q^c cut ranging from 0.25 to 30. The seed cut was set equal to the cluster cut so that no additional selection was

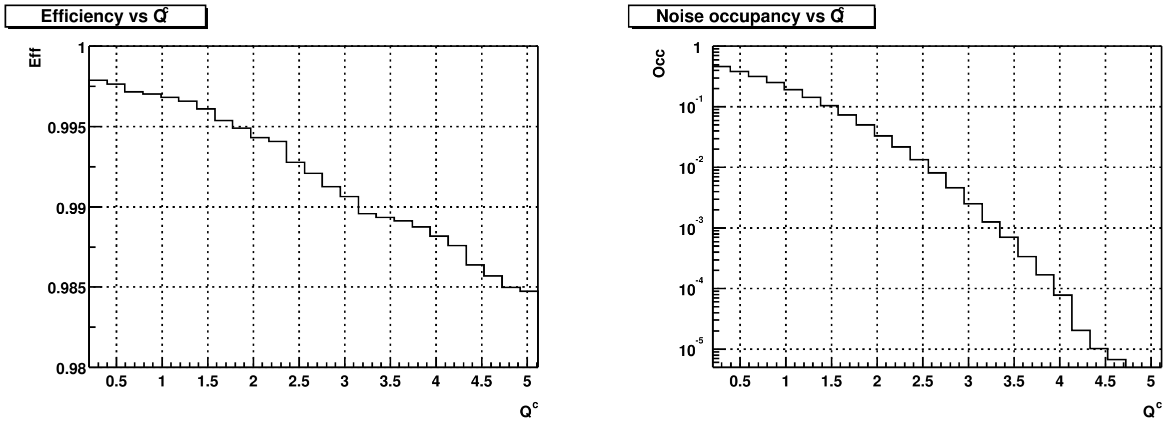

Figure 2.7: Example of efficiency and noise occupancy versus Q^c cut ($\theta = 0°$, 6cm strips).

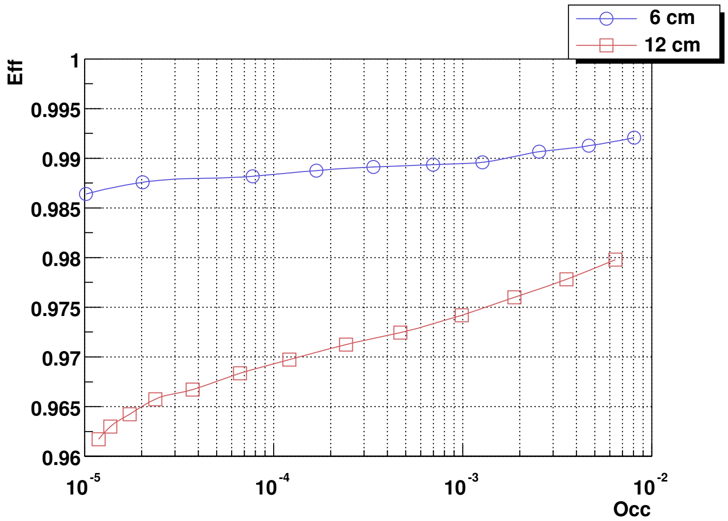

Figure 2.8: Efficiency versus noise occupancy for 6 and 12 cm strips ($\theta = 0°$).

requested. For a cluster to be considered efficient, the track intersection had to lie within the boundaries of the cluster. The minimum signal cut was also imposed on the matching cluster ($S^{min} = 50\,\mathrm{mV}$ for 6 cm strips and $S^{min} = 70\,\mathrm{mV}$ for 12 cm ones) so as to assure that the cluster was not due to a noise. See Fig:2.7 for the two plots. Then these two were combined to give the `efficiency versus occupancy` graph which is the standard representation. Fig:2.8 shows the results.

Now is the time to define the clustering cuts that will be used in the later analysis. The clustering cut Q^c and the seed cut Q^s are set to 3 and 4 respectively. This ensures that the noise occupancy stays below 5×10^{-4} (requirement for the ATLAS SCT) while still allowing the cluster to contain the boundary strips which receive only small quantities of charge. The minimal signal cut was $S^{min} = 50\,\mathrm{mV}$ for the 6 cm detectors and $S^{min} = 50\,\mathrm{mV}$ for the 12 cm detector. For the maximal signal cut the value of $S^{max} = 1000\,\mathrm{mV}$ proved to be adequate as there were some read-out errors which resulted in a signal readings above 1200 mV, while the highest signals collected at $\vartheta = 50°$ were not larger than 800 mV. $\mathcal{N}^{min}$ and $\mathcal{N}^{max}$ vary with the inclination of the detector so as to cover all expected cases (with a reasonable tolerance on each side).

2.5.2 Resolution

The beam telescope enables one to predict the track crossing position with a resolution of 2.5 μm. By comparing the measurements taken by the test detector (and using one of the position correction algorithms) to the predicted value one obtains its resolution. The distances are always calculated in the detector's plane. For $\theta = 0°, 10°$ there are mainly one–strip clusters present. For those only the `centre of gravity` method was used (which is equivalent to taking the strip's centre). For clusters of a larger size, the `eta` and `analogue head-tail` methods were also used.

Fig:2.9 compares the residual distributions for one strip clusters (where `centre of gravity` method was used) and for two strip clusters (`eta` method). The interesting thing to notice is that the single strip cluster resolution is improved at 10° as two-strip clusters are produced by the tracks close to the strip boundary.

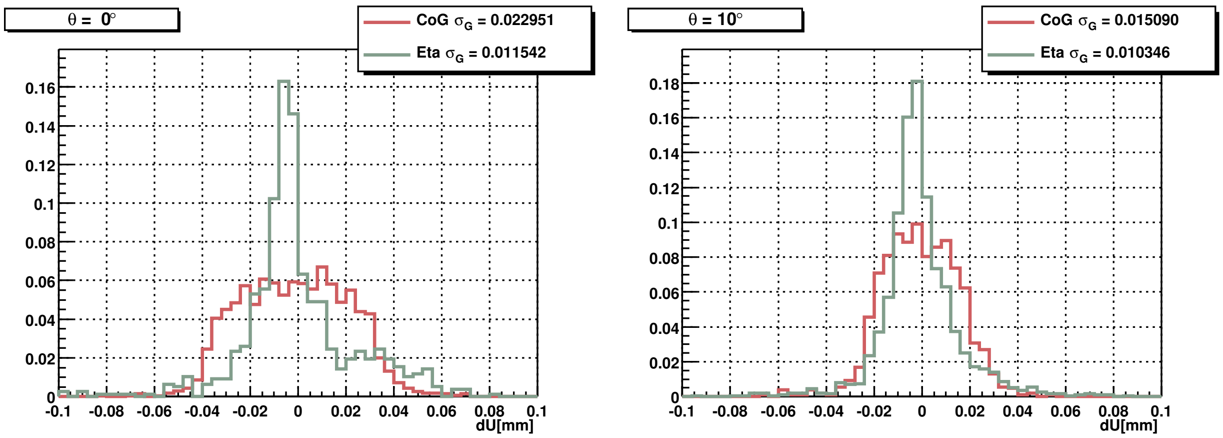

Figure 2.9: Comparison of residual distributions for one (red) and two-strip (green) clusters. Shown for 6 cm detector at $\theta = 0°$ (left), 10° (right).

Figure 2.10 shows the resolutions obtained with different methods as a function of the inclination of the detector. Single strip clusters have been omitted in this analysis. As expected, the `eta` method gives the best results for small inclinations (0° and 10°). The `analogue head-tail` method provides only a slight improvement compared to the `centre of gravity` method. For 6 cm and 12 cm detectors the best resolution can be obtained at 10°. For higher inclinations the resolutions degrade as the signal per strip gets smaller and its signal to noise ratio is reduced. This can also be observed by comparing the resolutions of the 6 cm detectors to those of the 12 cm ones for which the noise per strip is about 1.4 times larger.

2.5.3 Cluster size, signal and signal to noise

A particle passing through the detector creates electron–hole pairs in the semiconductor. Drifting charge then influences the voltage applied to the read out strips which are coupled capacitively to the electronics. Ideally one would expect that all the charge produced in the region covered by a single strip (that is the strip centre $\pm\frac{P}{2}$) gives rise to a signal on this strip only. But the finite collection time and charge diffusion cause the charge produced close to the two strip boundary to be distributed among both strips. Cluster size is the first measure of charge sharing, a detailed study of which is the subject of the next section.

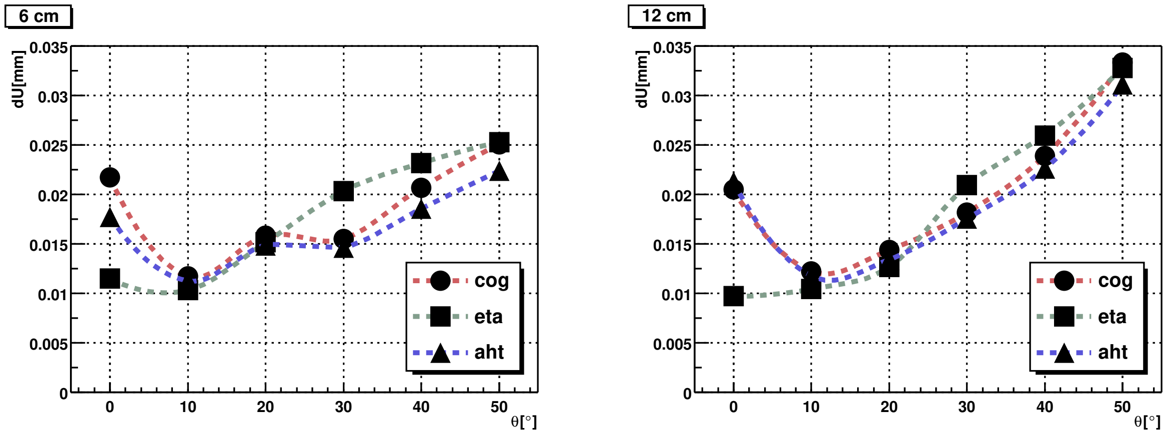

Figure 2.10: Sigma of Gaussian fit to residual distribution versus angle for different position correction methods. Clusters with at least two strips were used.

The cluster size is dependent on the inclination of the detector (see Fig:2.6 as a guideline). To estimate the cluster size, consider the projected track length on the detector plane in a direction perpendicular to the strips:

$$a = W \tan\theta. \tag{2.17}$$

Then there are two effects: the first one is rather artificial as it is introduced by the Q^c clustering cut. It truncates the effective length of tracks that cover a short distance under the region of the bordering strips. Effectively this reduces the thickness of the active region. The second effect is caused by charge diffusion which increases the cluster size and is independent of the inclination angle. All things considered, the average expected cluster size is:

$$\mathcal{N}_c = 1 + \frac{(W - w_c)\tan\theta + d}{P}, \tag{2.18}$$

where w_c is the effective width of the layer suppressed by the Q^c cut and d is the average charge diffusion length perpendicular to the strips. The dependence of the cluster size as a function of the inclination angle was then fitted with this function. The results obtained for the test detector are given in Fig:2.11. The loss of active area is larger for 12 cm detector as expected with the higher noise. The diffusion lengths are consistent.

Closely connected to cluster size is the distribution of the total signal collected in a cluster. Theoretically, for thin absorbers, given certain distance through the sensitive material, one finds that the signal follows the Landau distribution (see [18]):.

$$\Phi(\lambda) = \frac{1}{\pi}\int_0^\infty e^{s\log s - \lambda s}\sin\pi s \, ds, \tag{2.19}$$

$$\lambda = \frac{S^c - S^{\mathrm{MP}}}{\sigma_{\mathrm{L}}}. \tag{2.20}$$

The Landau distribution has two parameters: S^{MP} is the most probable signal (peak position) and σ_{L} is a width of its Gaussian core. Both increase with the thickness of the material. In practice, this distribution is effectively convoluted with a Gaussian of σ_{G}. Effectively this is the average signal fluctuation in a cluster due to a noise. Cluster signal S_C was histogrammed

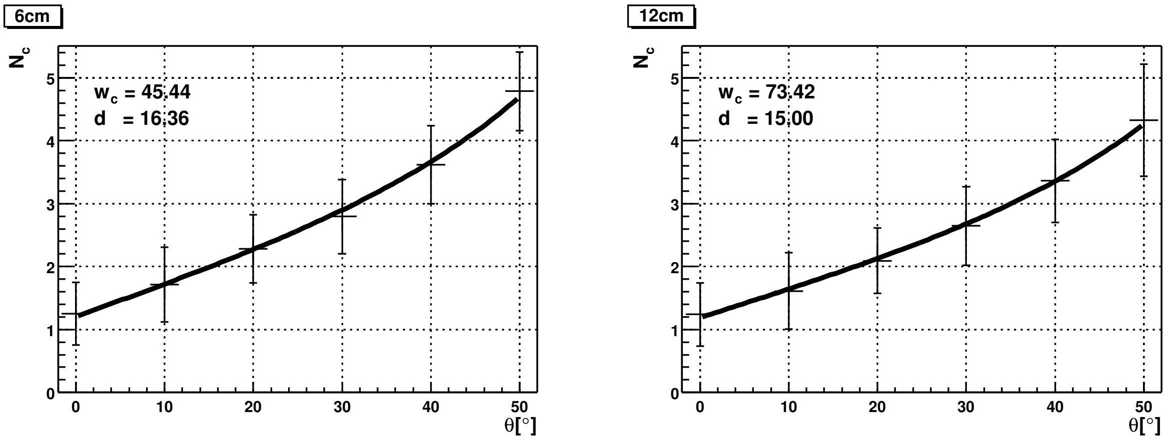

Figure 2.11: The cluster size for 6 cm (left) and 12 cm (right) detectors. The error bars show rms's of the distributions. The results of a fit to Eq:2.18 are superimposed on the plots.

for different angles and detector lengths and fitted to a convolution of Landau and Gaussian distributions. Figures 2.14 and 2.15 present the results (both figures can be found at the end of this chapter). As inclination increases a surplus of events in the high-signal tails of the distributions can be observed. These are caused by the δ-electrons.

For the most probable cluster signal, the relevant quantity is the track length through the sensitive material:

$$l = \frac{W}{\cos\theta}, \quad S_C^{\mathrm{MP}} \propto l. \tag{2.21}$$

To get a better estimation of the most probable signal per particle per distance travelled, the S^{MP} obtained from the Landau fits was plotted versus the angle and the points fitted with $S_0^{\mathrm{MP}}/\cos\theta$. Fig:2.12 shows the dependence of the most probable cluster signal $S^C(\vartheta)$ and results of the fit. Since 21 000 electron-hole pairs is the most probable yield for a minimum ionizing particle in 280 μm thick silicon layer and the signal amplification is linear, we can calculate the calibration constant to be 7.5 mV per 1 000 electron-hole pairs.

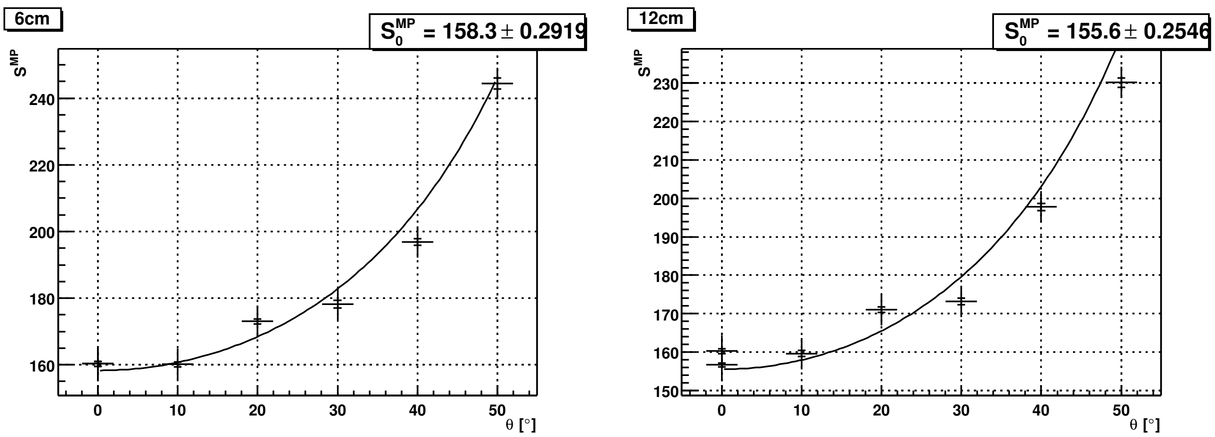

Figure 2.12: The most probable signal S^{MP} as a function of θ for 6 cm and 12 cm detectors. For both plots the fits to eq:2.21 are superimposed.

Another measure of a cluster's quality is its signal to noise ratio, defined in Eq:2.9. Fig:2.13 gives its dependence on the inclination of the detector. The average value of Q_C for the 6 cm detector is, on average, 1.3 times larger than that for the 12 cm one. By assuming that the noise of the electronics is constant and that the capacitive noise of the 12 cm detector is twice that of the 6 cm one, relative contributions from the electronics and detectors to the total noise can be estimated. The average number of electron-hole pairs produced (30 200) is also needed to extract the absolute values. The noise of the electronics 'measured' this way corresponds to the equivalent noise charge of $ENC_e \sim 730$ electron-hole pairs and that for the 6 cm detector to $ENC_{6\,\mathrm{cm}} \sim 390e^-$.

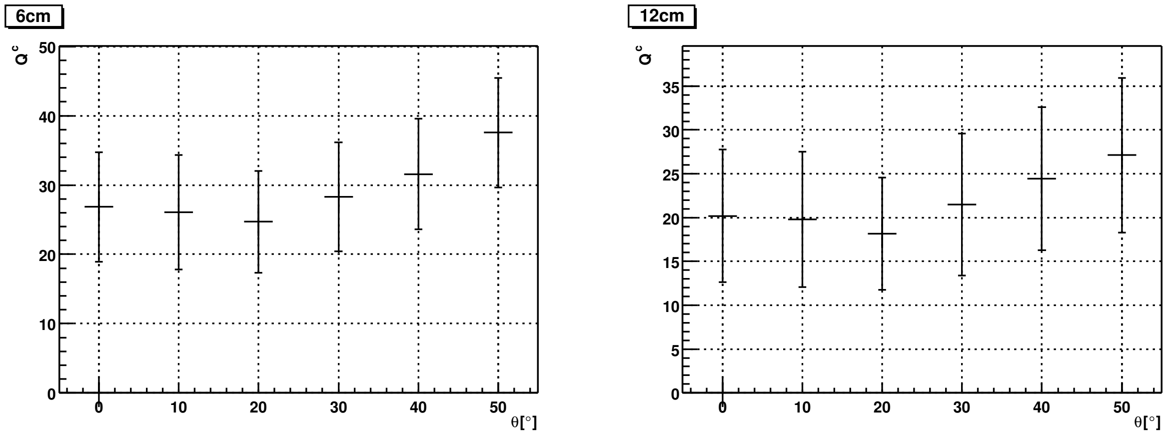

Figure 2.13: The mean value of cluster's signal to noise Q_C as a function of θ for 6 cm and 12 cm detectors. The error bars show rms's of the distributions.

2.5.4 Collected charge distribution

We are interested in how the charge gets distributed over the sensitive material. Having a cluster and knowing the intersection position, we can enter points representing each strip in two dimensional histogram. The charge fraction S_i/S_C was plotted versus the distance of the strip center from the intersection point in the detector plane (Figs. 2.16 and 2.18). A clearer picture but somewhat stripped of information can be obtained by profiling the histogram in the S_i/S_C axis and showing just the mean and rms versus distance (Figs. 2.17 and 2.19).

In these distributions one can notice a slight tendency for the strip signal increase, as we go toward higher strip indexes. This was introduced into the measurements by a malfunctioning ADC in the data acquisition system, which caused about 10% of a channel's signal to be sporadically added to its successor. This channel cross-talk has been reproduced afterwards but, unfortunately, no regular pattern has been observed that would enable it to be eliminated from the collected data.

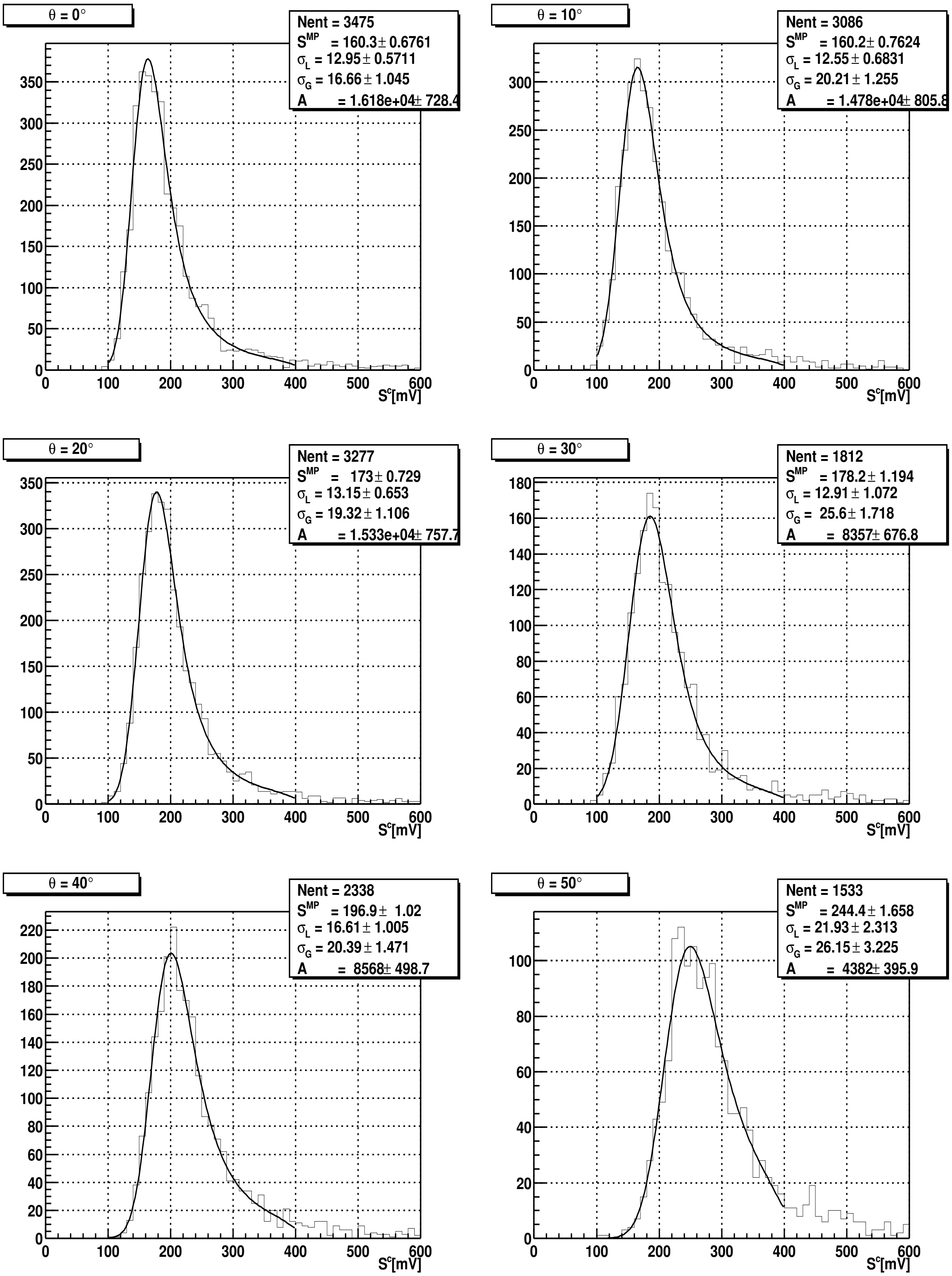

Figure 2.14: Distributions of the reconstructed signal with superimposed Landau fit in a range 100-400 mV for 6 cm detectors at different angles. Parameter A is the normalization constant.

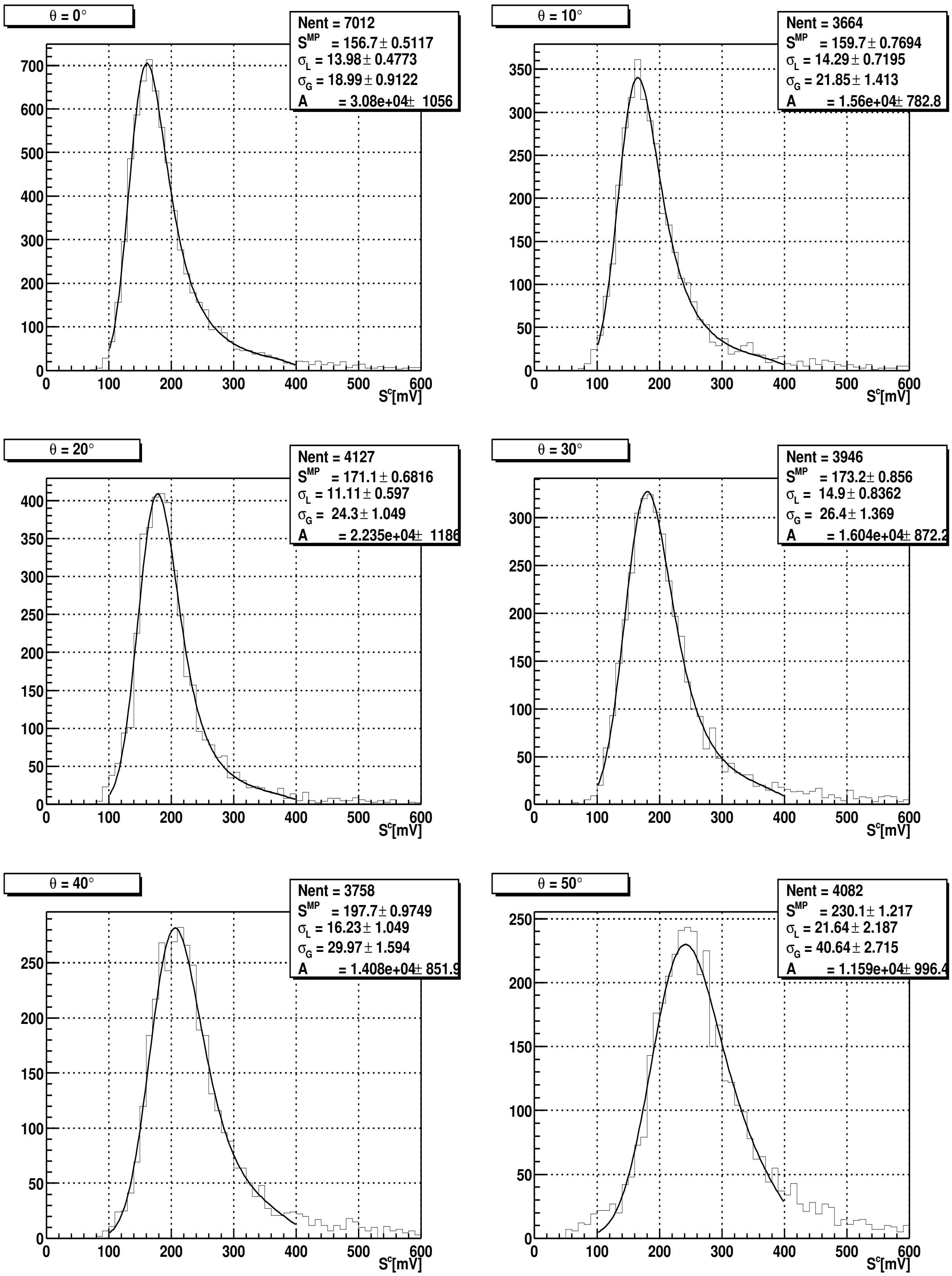

Figure 2.15: Distributions of the reconstructed signal with superimposed Landau fit in a range 100-400 mV for 12 cm detectors at different angles. Parameter A is the normalization constant.

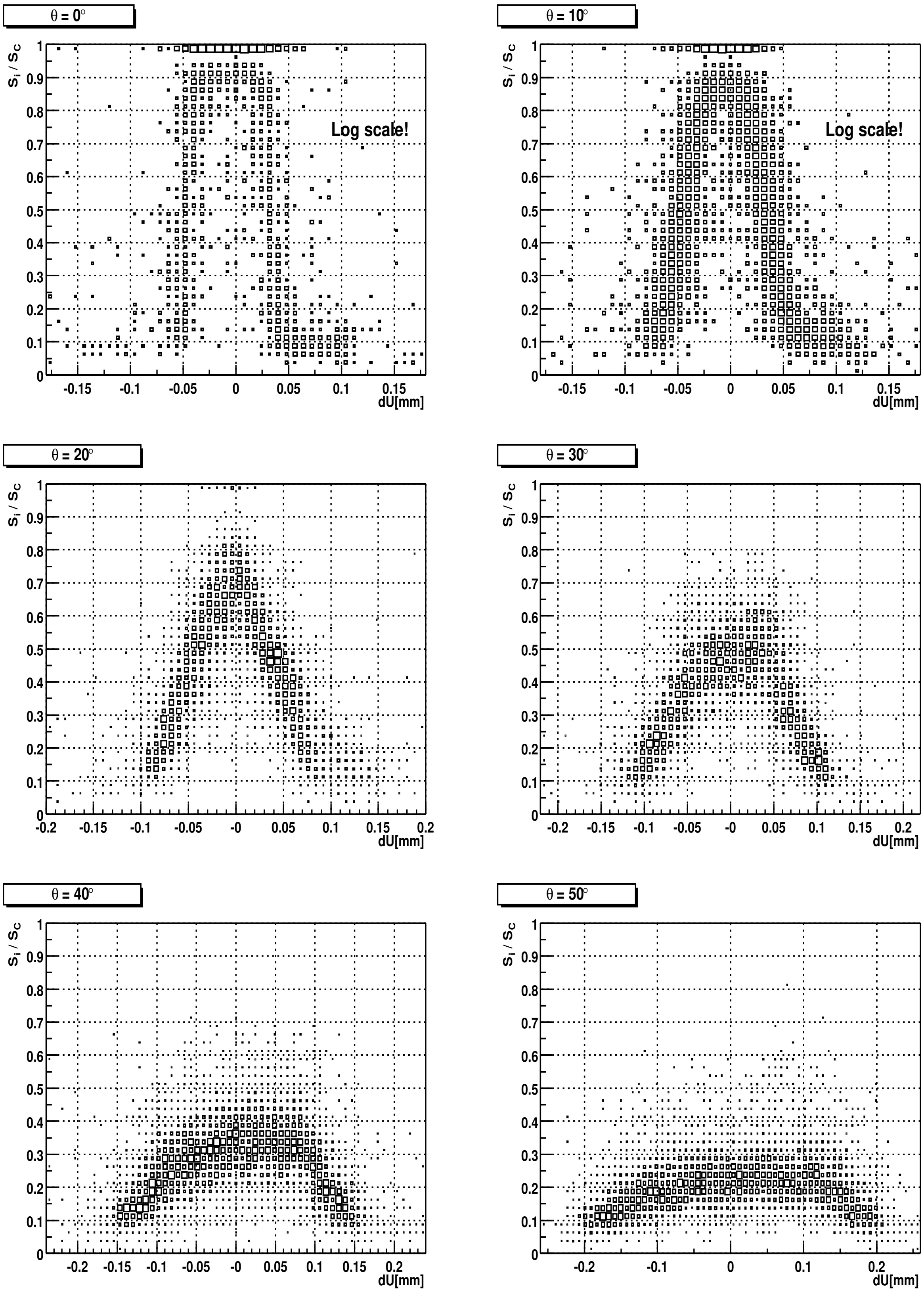

Figure 2.16: Collected charge distribution for 6 cm detectors at different angles. The z axis is logarithmic for $\theta = 0^\circ$, 10°.

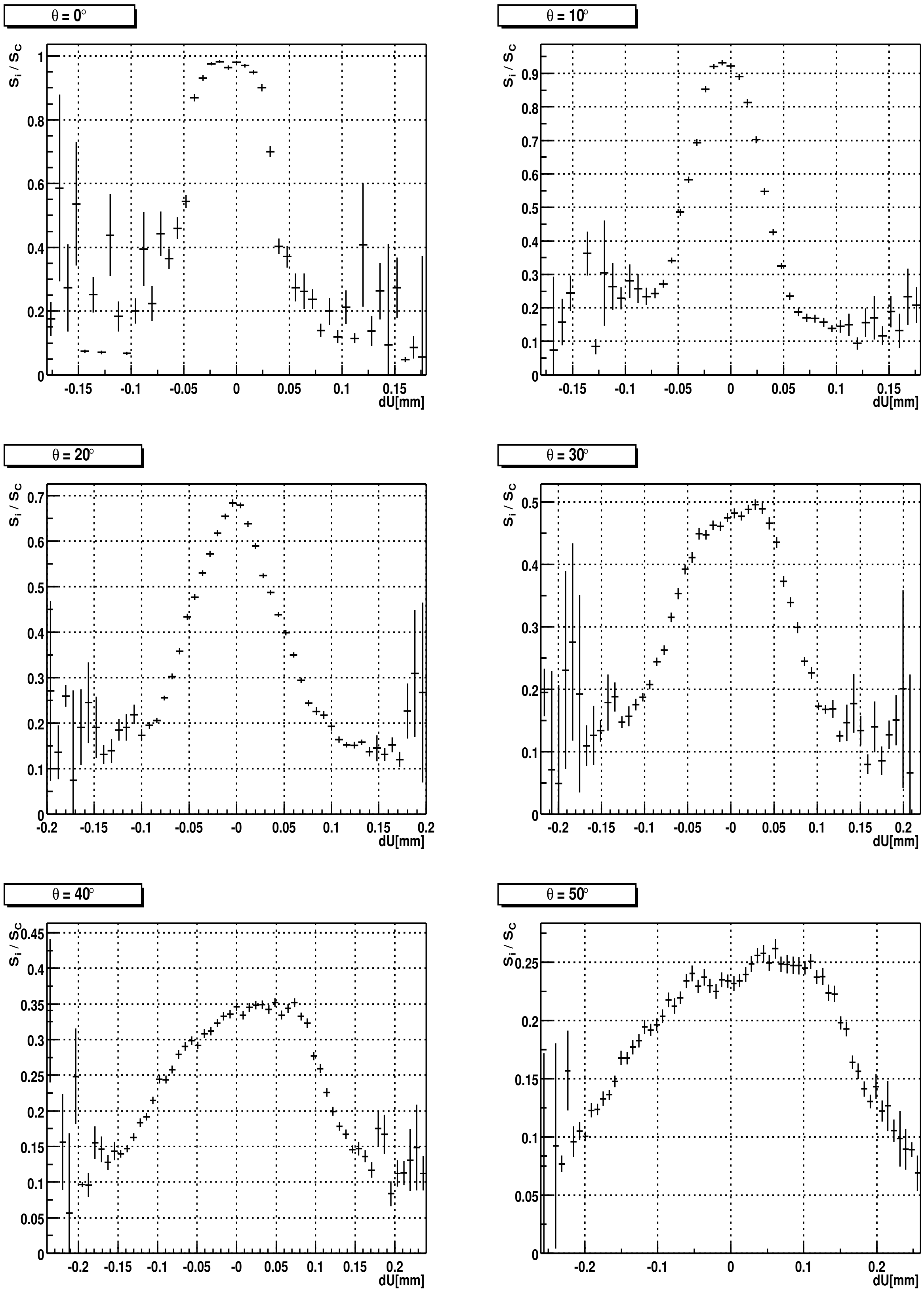

Figure 2.17: Collected charge distribution for 6 cm detectors at different angles shown as profiles.

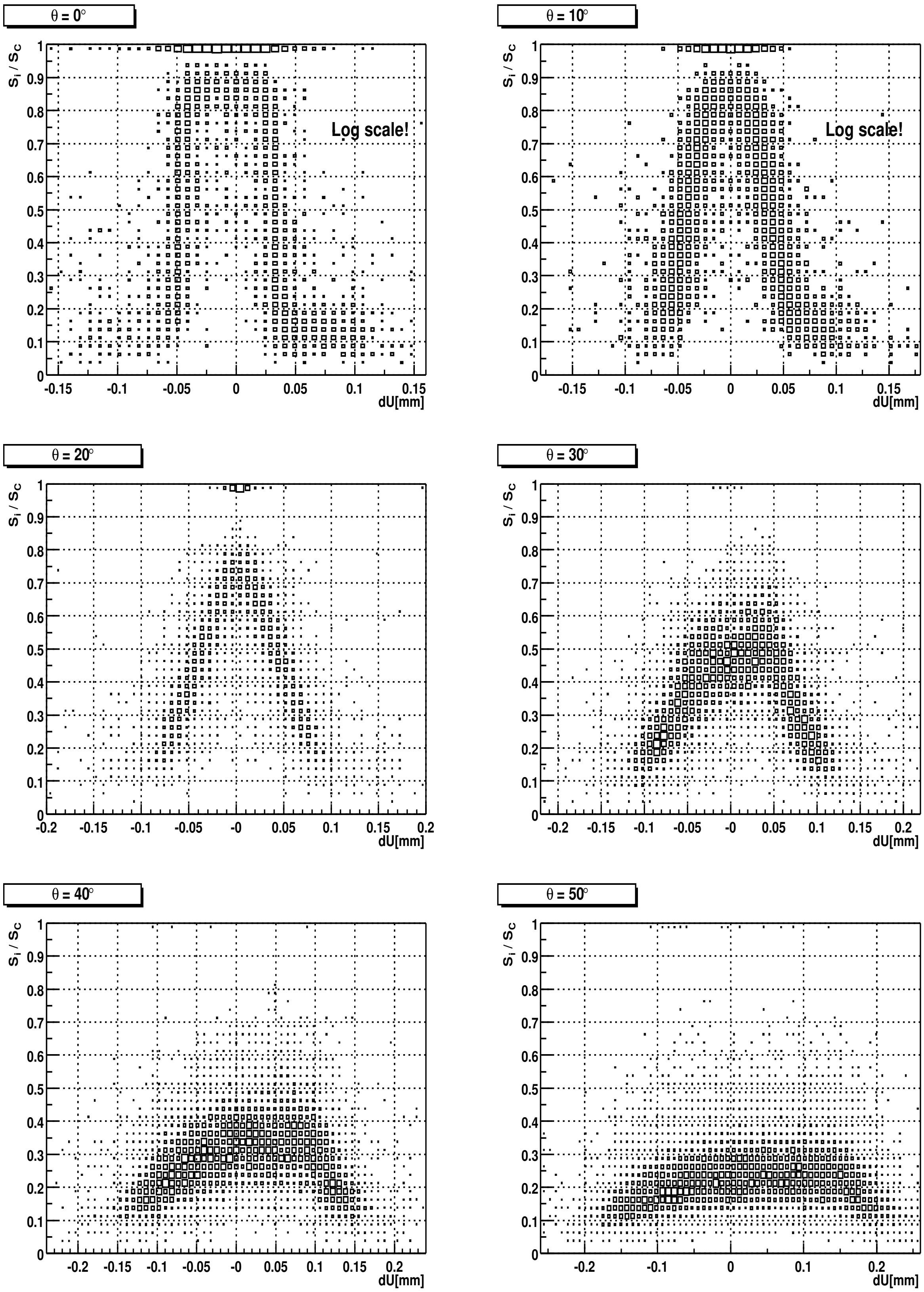

Figure 2.18: Collected charge distribution for 12 cm detectors at different angles. The z axis is logarithmic for $\theta = 0°$, $10°$.

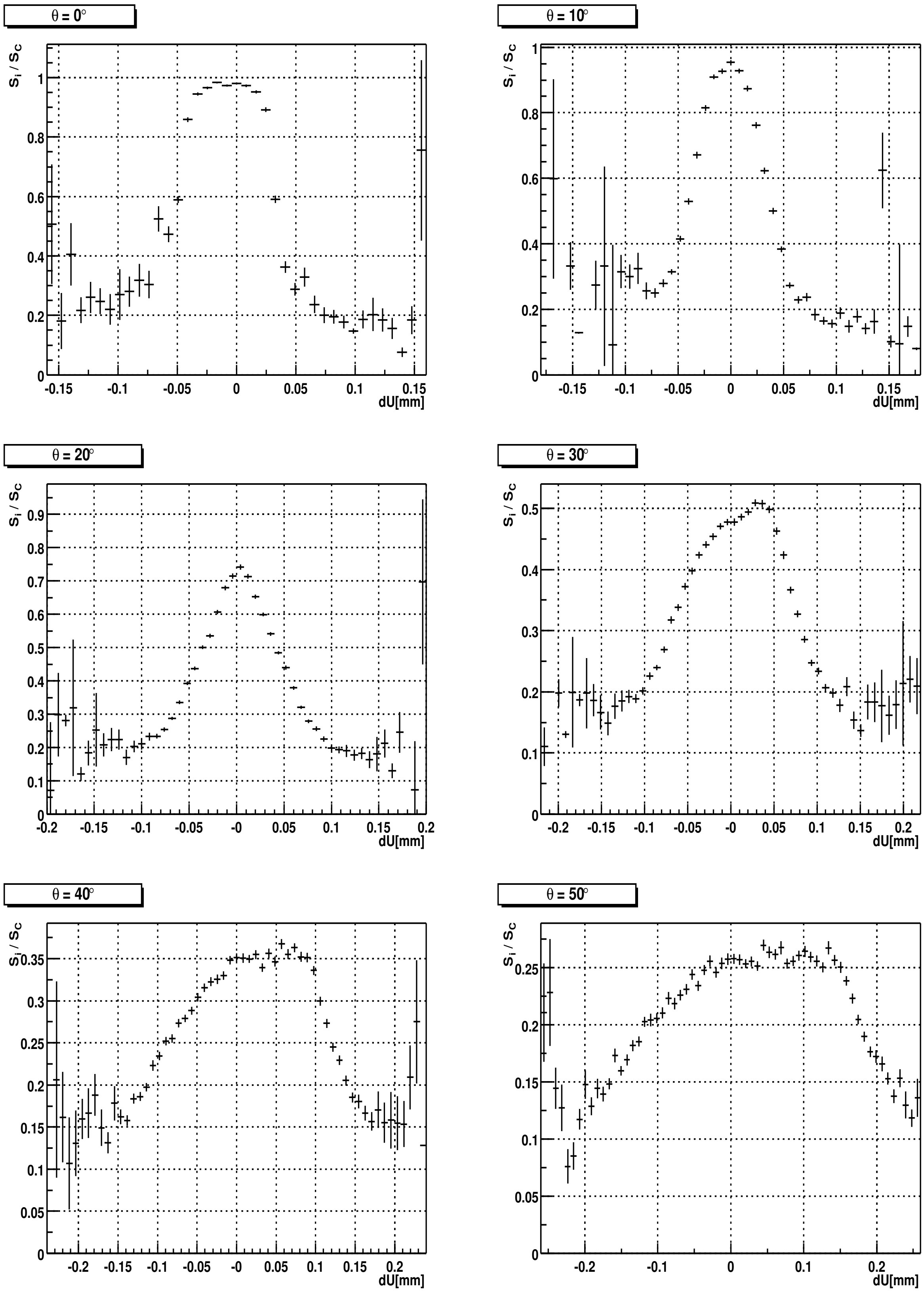

Figure 2.19: Collected charge distribution for 12 cm detectors at different angles shown as profiles.